

Available online at www.sciencedirect.com

ScienceDirect

journal homepage: www.elsevier.com/locate/he

Localized surface plasmon resonance (LSPR) detection of hydrogen gas by Pd²⁺/Au core/shell like colloidal nanoparticles

Ameneh Farnood, Mehdi Ranjbar*, Hadi Salamaty

Department of Physics, Isfahan University of Technology, Isfahan, 8415683111, Iran

HIGHLIGHTS

- Gold nanoparticles (GNPs) were fabricated by pulsed laser ablation (PLA) method in DI water.
- PdCl₂ solution with different concentration was added to the obtained GNPs colloidal solutions.
- TEM showed Pd²⁺/Au and single NPs before and after hydrogen injection, respectively.
- The Au LSPR peaks in Pd²⁺/Au system undergoes spectral shift during the gas injection.
- Au LSPR shift was used for detection of the hydrogen concentration below 4%.

ARTICLE INFO

Article history:

Received 3 August 2019
Received in revised form
23 September 2019
Accepted 20 October 2019
Available online xxx

Keywords:

Gold nanoparticles
PdCl₂
Localized surface plasmon
resonance
Hydrogen sensing
TEM
XPS

ABSTRACT

A hydrogen detector colloidal solution based on the plasmonic properties of gold nanoparticles (GNPs) is presented. GNPs were prepared by pulsed laser ablation (PLA) of gold target in DI water. PdCl₂ solution with different concentration was added to the obtained GNPs colloidal solutions. X-ray diffraction (XRD) confirmed the formation of metallic gold and presence of PdCl₂ phases. Transmission electron microscope (TEM) images along with X-ray photoelectron spectroscopy (XPS) revealed formation of the core-shell-like structures of Pd²⁺/Au NPs. After hydrogenation, TEM revealed that the core-shell morphology changes into free NPs and XPS revealed formation of the metallic Pd phase. Voltammetry analysis showed a well absorption and desorption capability of hydrogen in this gold-PdCl₂ plasmonic system. After adding PdCl₂ aqueous solution, a red-shift from 522 to 526 nm was observed which was attributed to Pd²⁺ ion attraction by the negative surface charge of bare GNPs and formation a core-shell like morphology. The optical absorption peaks of PdCl₂ (the range 207–236 nm) as well as the LSPR peak of GNPs were traced during diluted hydrogen (0.3–10%) injection in colloidal samples with different Au:Pd molar ratio. It was found that the PdCl₂ peaks drop due to Pd²⁺ → Pd⁰ conversion and more importantly, the gold peak undergoes blue shift due to change in chemical properties of GNPs surrounding. A good correlation between PdCl₂ absorption intensity and gold LSPR peak position was found when hydrogen concentration was varied. In this correlation, a desirable detection capability for low concentrations of hydrogen (<4% range, the limit of hydrogen explosion) with a possible large number of points was observed. Finally, a model for the hydrogen sensing mechanism based on the LSPR effect was presented.

© 2019 Hydrogen Energy Publications LLC. Published by Elsevier Ltd. All rights reserved.

* Corresponding author. Department of Physics, Isfahan University of Technology, Isfahan, 841518311, Iran.

E-mail address: ranjbar@cc.iut.ac.ir (M. Ranjbar).

<https://doi.org/10.1016/j.ijhydene.2019.10.168>

0360-3199/© 2019 Hydrogen Energy Publications LLC. Published by Elsevier Ltd. All rights reserved.

Introduction

Hydrogen is a clean, renewable and sustainable source of energy that makes it suitable for the replacement of carbon-based energy sources which extensively used in fuel cells, medical applications, food industry and even in everyday heating and cooking [1,2]. Additionally, hydrogen is also being used widely in scientific research and industries, notably in the refining of petroleum products [3]. Hydrogen is strongly flammable at >4% concentration with a large flammability range (4–75%) [4]. Therefore, the detection of this explosive gas is very important compared to other gases [5,6]. For many years, palladium has been one of the important materials known to detect hydrogen gas due to its high sensitivity and selectivity and strong change of its optical properties towards hydrogen absorption [7,8]. After interaction with hydrogen, palladium converts from the metallic state to hydride states (α -phase at low H_2 content or β -phase at high H_2 content), which results in a lattice expansion up to several times the initial volume changes the conductivity and dielectric properties under ambient conditions [9–11]. The changes in dielectric property are very small and difficult to be measured, so we need a sensor with a high sensitivity to environmental changes. Hydrogen gas sensors based on optical properties of metal oxides [12–16] or noble metal [17,18] nanostructures provide an emerging powerful technique in chemical and biological sensing applications. Detection of H_2 in aqueous media such as water and chemical solutions is of crucial importance in environmental, biomedical sciences and biotechnology. Research on hydrogen-enriched fresh water and photochemical water splitting. For instance, hydrogen-enriched water has been reported to have a positive effect on human health [19]. Consequently, water-base liquid hydrogen indicator, particularly based on optical and visual devices can be of great interest for biological applications [20].

Interaction of light with metallic particles much smaller than the incident wavelength leads to localized surface plasmon oscillation with enhanced electromagnetic fields around a particle that is very sensitive to the variation in the dielectric properties of the analyte samples surrounding the noble metal nanostructures [21]. Mie originally calculated LSPR by solving the Maxwell's equations for small spheres with the certain boundary conditions, interacting with an electromagnetic field [22]. This theory provides the direct relationship between resonance wavelength and surrounding medium dielectric constant of nanoparticles.

Colloidal solutions of GNPs show a very intense color, which is not observed in the bulk material or in the discrete atoms [23,24]. Therefore, Au–Pd nanosystems can allow plasmonic sensing, which has advantages of high accuracy, no risk to generate sparks and not being affected by electromagnetic interference.

Various types of Au/Pd nanostructures have been demonstrated for plasmonic hydrogen sensing. Jiang et al. has reported ultrasensitive plasmonic sensing of hydrogen using bimetallic Au/Pd nanostructures with continuous and discontinuous Pd shells [5]. They observed a good linearity for LSPR wavelength and intensity with gas concentration with a 56 nm spectral shift in the presence of low concentration of

hydrogen. Rodal-C et al. has reported well-characterized seed-mediated grown Au@Pd nanorods with tuneable NIR LSPR response [25]. They compared hydrogen sensing in solution phase or on a substrate and demonstrated excellent reversible plasmonic properties for in situ monitoring of chemical reactions suitable for hydrogen detection. They also argued that Au support can boost the plasmonic properties of Au@Pd structure. In arrays of Pd–Au (Au content 0–25 atom %) alloy thin films prepared by lithographic technique have been used for plasmonic optical hydrogen sensing in which an 8-fold sensitivity enhancement was observed comparing to pure Pd at below hydrogen flammability limit [26]. Sugawa et al. have demonstrated Pd NPs as third plasmonic sensing material in which a dipole mode creates in the presence of Au core leading to refractive index susceptibility higher than bare Au NPs [8]. In a paper by Wy et al., colloidal clusters of Au@Pd bimetallic NPs have been reported as a LSPR sensing platform for hydrogen gas in aqueous phase. They attributed the observed highly sensitivity for hydrogen detection to promoted plasmonic field due to cluster formation [27]. They stated that manipulation of Pd shell thickness can increase the LSPR hydrogen sensitivity. Polyhedral Au nanocrystals covered by an epitaxial layer of Pd have been used for hydrogen detection in aqueous solutions based on plasmonic resonance absorption [28]. The gold cores as effective plasmonic antenna were responsible for hydrogen detection at low percent with a very large red shift in the presence of dissolved hydrogen in water. Moreover, no spectral shift has been observed in the presence of oxidant gases such as Co and oxygen. In 2018, Song et al. were reported films made simply by centrifugal deposition of Au–Pd core-shell NPs and observed optical detection of hydrogen with few 10 s repose time for 4% hydrogen [29]. Co-sputtered Au and Pd films have been used for hydrogen storage where hydrogen uptake and release rate were measured by optically monitoring of extinction loss [30]. Recently we have introduced Pd–MoO₃ colloidal solution as an LSPR hydrogen sensing platform in aqueous phase where a good sensitivity with possible large number of points was observed [20].

The brief review of the above articles shows that Au–Pd nanostructures have high potential for detecting hydrogen on the basis of plasmonic properties of gold (and even palladium) in which accuracy, sensitivity, response speed and safety are promising. However, their production methods sometimes require film deposition or lithography equipment to allow make a proper connection between the two phases. All of these articles also use metallic palladium, while Pd²⁺ cations not only have the ability to oxidize hydrogen, they can also be physically absorbed by the negative surface charges of gold nanoparticles and form weak shell states. It is expected that hydrogen adsorption reduce these ions, convert them to metallic phase and affect the dielectric properties of gold nanoparticles and provide a plasmonic based method for hydrogen detection. Another advantage of this is the simplicity and cost-effectiveness of the fabrication methods by simply combination of aqueous palladium salts and colloidal gold nanoparticles. To our best knowledge, no articles exist on plasmonic hydrogen sensing of Pd²⁺–Au system hence exploring this subject is of scientific importance.

Pulsed laser ablation in liquid is an outstanding approach for producing gold nanoparticles that have unique properties such as high purity, surface functionality, and the formation metastable states [31,32]. In this paper, in spite of last works that investigated Au–Pd as a bimetallic, core-shell or thin film, we simply mixed GNPs and PdCl₂ colloidal solutions and examined their plasmonic response to low concentration of hydrogen in room temperature. Our previous works indicates a weak core/shell structure of palladium and gold due to the negative surface charge of GNPs [33]. Herein, the role of adding PdCl₂ solution as a dielectric medium is investigated which is very sensitive to the presence of hydrogen and was successfully applied to LSPR detect hydrogen gas. In this work, we use laser ablation for synthesis gold nanoparticles and then PdCl₂ solution added in different ratios. We have fabricated and tested five different Au–Pd colloidal solution for hydrogen sensing and examined their plasmonic response to H₂ gas by tracking the absorption spectra of the samples. The presented structural, morphological, surface analysis, electrochemical reactions and optical properties were studied by using XRD, TEM, XPS, cyclic voltammetry and UV-Vis spectrophotometer, respectively.

Experimental

The schematic representation of sample preparation is depicted in Fig. 1. GNPs were prepared by laser ablation in DI water medium. Au target (99.99%, PAMP S.A. Switzerland) was placed in the glass vessel filled with deionized water (200 ml) and a beam from an Nd:YAG laser ($\lambda = 1064$ nm, energy per pulse = 600 mJ, R.R = 9 Hssz) was focused normal to the

surface of Au target. The ablation was performed until the solution obtained a deep red color (30 min). The concentration of the GNPs was determined by inductively coupled plasma (ICP) optical emission spectrometer (20.21 mg/l). The PdCl₂ solution, as Pd²⁺ precursor, was prepared by dissolving 0.02 g of palladium (II) chloride ((59% Pd) Merrck Schuchardt OHG) powder into a combination of 0.1 cc HCl and 99.9 cc DI water. This composition was kept in ultrasonic bath until PdCl₂ was dissolved and a uniform yellowish solution was obtained after 1 h. The concentration of the PdCl₂ solution was determined by ICP analysis (223.20 mg/l). The pure Au and PdCl₂ as reference samples and physical mixture of PdCl₂ and GNPs with different ratios, were prepared and labelled as Au, PdCl₂, Au₈Pd₁, Au₆Pd₁, Au₄Pd₁, Au₂Pd₁, Au₁Pd₁ and Au₁Pd₂ (Table .1). In all samples the amount of GNPs is fixed and only PdCl₂ concentration was changed. The crystalline structures of nanoparticles were determined using X-ray diffractometer (Philips EXPERTMPD) with Cu-k α ($\lambda = 0.15418$ nm) radiation in 2 θ range of 10–80°. For this characterization, samples were prepared by drop-casted over glass substrates. The morphology and size of our nanoparticles were investigated by TEM model Philips CM120. X-ray photoelectron spectroscopy (XPS) was carried out using an ESCA/AES lab where a concentric hemispherical analyser (CHA, Specs model EA10 plus) has been used for photoelectron energy analysing. The electrochemical experiments were performed using a standard three-electrode electrochemical cell through an Ivium-stat Potentiostat at ambient temperature. Glassy carbon plates (1 × 1 cm²) were used as working electrodes, Ag/AgCl (sat. KCl) and a Pt wire were used as the reference and counter electrode in 0.5 M H₂SO₄ as the electrolytic solution. The cyclic voltammetry (CV) measurements were conducted in –0.2 to

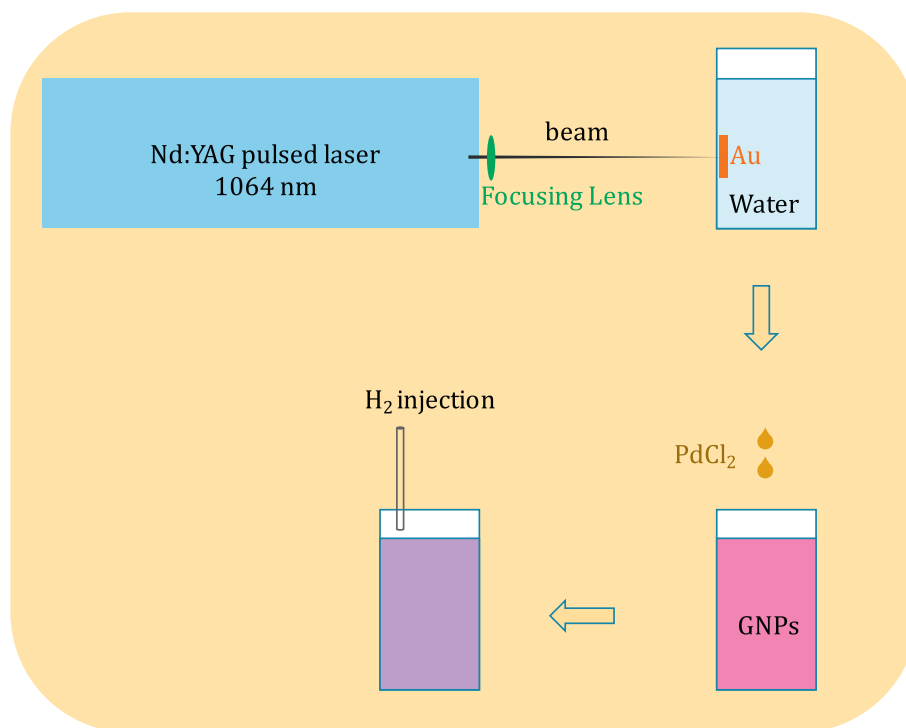
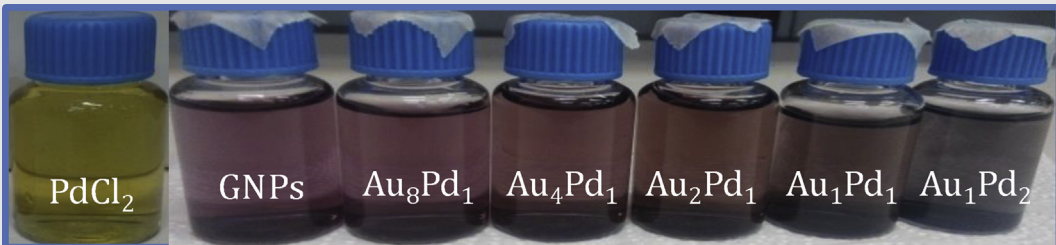


Fig. 1 – Schematic demonstration of AuPd colloidal NPs preparation. GNPs are fabricated by Nd:YAG laser ablation of Au target in DI water and PdCl₂ solution is dropped with different concentrations. Then hydrogen gas with various concentration is injected and the optical variation of colloidal samples are recorded.

Table 1 – Name of samples and its Au:Pd ratio. Bottom shows the photographic images of colloidal solutions.

| Sample | PdCl ₂ | Au | Au ₈ Pd ₁ | Au ₄ Pd ₁ | Au ₂ Pd ₁ | Au ₁ Pd ₁ | Au ₁ Pd ₂ |
|---------|-------------------|-------|---------------------------------|---------------------------------|---------------------------------|---------------------------------|---------------------------------|
| (Au:Pd) | (0:1) | (1:0) | (8:1) | (4:1) | (2:1) | (1:1) | (1:2) |



1.2 V potential range. CV of samples was carried out at a scan rate of 50 mV s⁻¹. The synthesized samples were drop-coated over a polished glassy carbon electrode (GCE) at room temperature. Optical properties of samples were measured by using a Lambda 25 spectrophotometer (PerkinElmer) in the 190–1100 nm range with 1 cm optical path length. The resolution of the spectrometer is 0.1 nm. LSPR Hydrogen sensing tests were performed by using a 100 ml glass bottle at room temperature. During the experiment, solutions were being stirred.

A volume of 20 ml of Au–Pd solution was used for the experiment. The glass bottle was evacuated prior to the hydrogen injection in order to remove the existing air for 30 s. The hydrogen was injected using a syringe filled with hydrogen of different concentrations mixed with Ar gas for 10 min. Then UV–Vis absorption spectrum of this solution was recorded.

Results and discussions

XRD

XRD patterns corresponding to Au and Au₁Pd₂ samples are shown in Fig. 2(a and b), respectively. The XRD pattern of Au sample (part (a)) depicts the Au (111), (200), (220) and (311) diffraction peaks which are associated to crystallographic orientations of gold cubic structure (JCPDS no. 00-001-1172). Therefore, GNPs have been formed successfully in the laser ablation process of gold target in DI water. The addition of PdCl₂ solution to the colloidal GNPs leads to appearance strong (101), (110) and (520) diffraction peaks of rhombohedral PdCl₂ phases (JCPDS no. 01-086-1888). Similar phases were observed for gold and palladium chloride in other samples. The diffraction peak of Au are relatively weak, suggesting that palladium is likely to surround the GNPs and prevent them from sticking together, resulting in no effective X-ray diffraction [33]. This prediction will be confirmed later by TEM images.

It should be noted that when large amounts of colloidal samples are dried prior to the XRD analysis, it may be different from how the phases are stacked together in the colloid state. Therefore, analyses, such as TEM and XPS that require less amount of the material, are more accurate. Therefore, for further study, these analyses are also used.

TEM images

Since for plasmonic-based sensing of hydrogen, the shape and how GNPs are attached to the PdCl₂ surrounding are important factors, the TEM images of the samples were studied. The TEM image and corresponding size distribution histogram of pristine GNPs (sample Au, Fig. 3(a)) represents spherical shape particles with 8.6 ± 2 nm average size. After adding the PdCl₂ solution to these spherical nanoparticles (sample Au₁Pd₂, part (b)), one can see formation of new agglomerates at the surface of GNPs. These agglomerates are constructed from very fine palladium phase particles that completely cover the GNPs and form core-shell like structures. The formation of these agglomerates was also observed in other ratios in which shell thickness increased with increasing Pd²⁺ concentration. It can be recognized that this palladium agglomerates separate the GNPs from each other and this is probably the reason for the weakening of the gold-diffraction peaks in the sample Au₁Pd₂. However, after hydrogen exposure, these agglomerates and their constructing fine particles are no longer observed (sample Au₁Pd₂ part (c)). According to the size distribution histograms, the size of the GNPs, before and after hydrogen

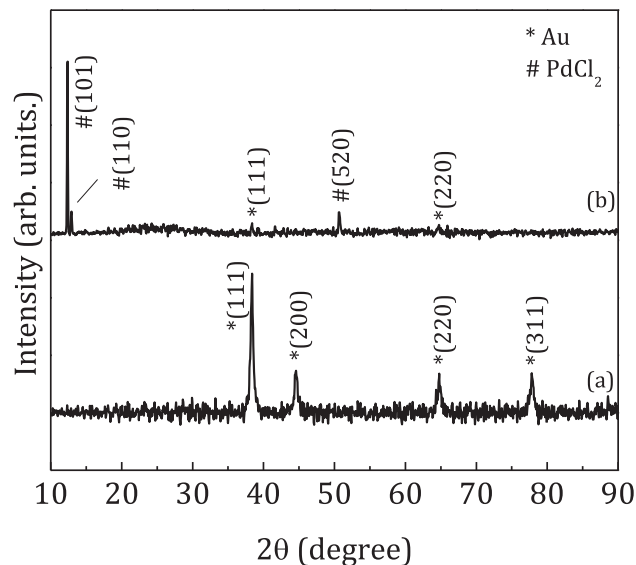


Fig. 2 – XRD patterns of (a) pristine GNPs (sample Au) and (b) sample Au₁Pd₂.

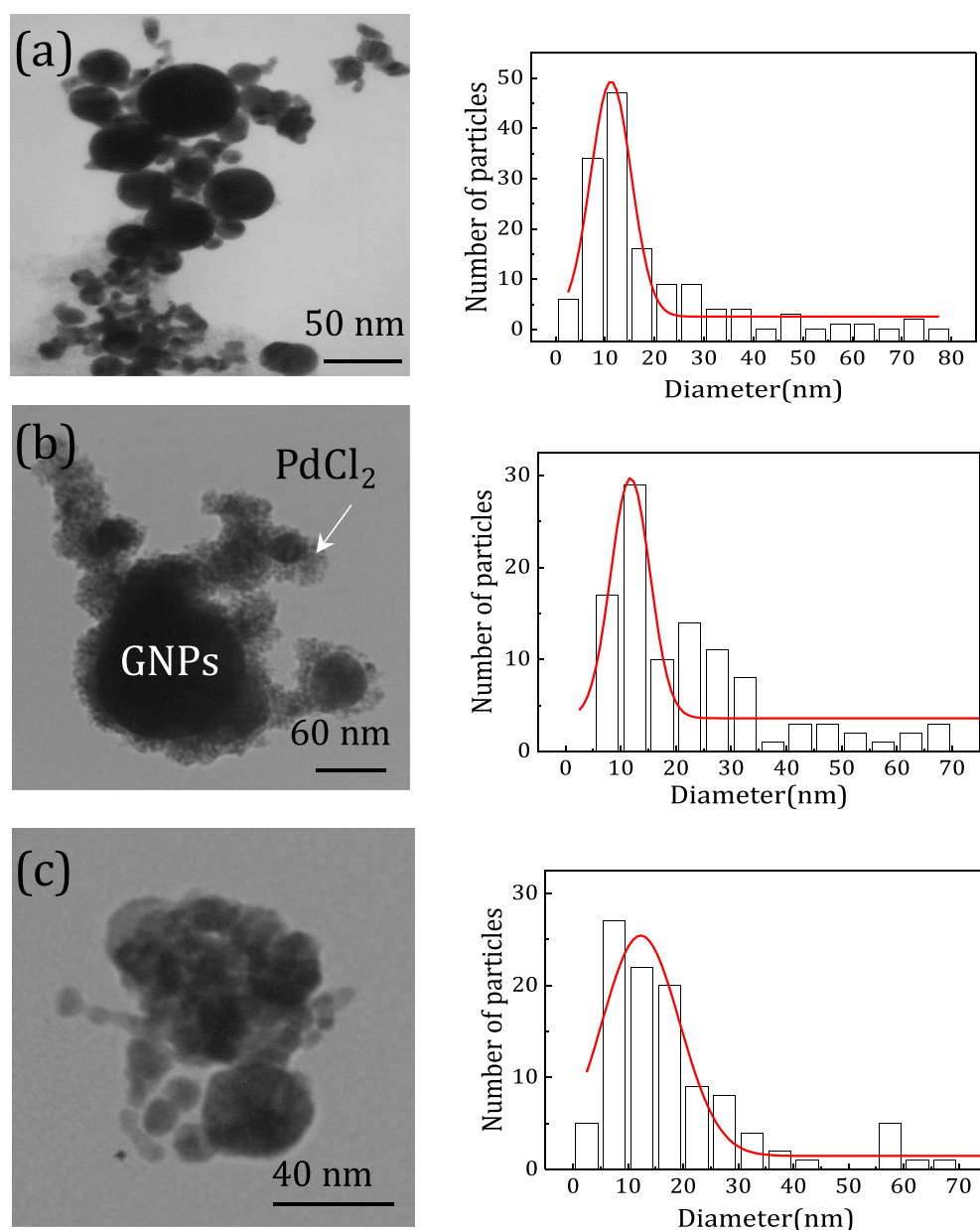


Fig. 3 – TEM images and corresponding size distribution histograms of (a) GNPs, (b) Au₁Pd₂ sample before and (c) after 10% H₂ exposure.

exposure, remains almost unchanged (around 10 nm) compared to the pristine Au sample, while palladium agglomerates were removed from the GNPs and are no longer observed in the form of shells. Accordingly, plasmonic properties of the colloidal GNPs are expected to undergo several spectral shifts as a result of PdCl₂ attachment to and removal from the GNPs after hydrogen exposure.

XPS

The chemical compositions of drop-casted pristine GNPs (sample Au) and sample Au₁Pd₂, before and after hydrogen exposure, were analysed by using XPS. Fig. 4 displays the high resolution XPS spectra at 330–346 eV region involving both

Pd_{3d} and Au_{4d} core level transitions. For pristine GNPs, a broad single-peak located at 335.1 eV with FWHM of 4.2 eV is observed. This broad core-level peak is attributed to the metallic gold (Au⁰) [34], in consistent with XRD results. After treatment with the PdCl₂ solution and before hydrogen injection, Pd_{3d} doublet appears at 343.3 and 383.1 eV which is related to Pd²⁺ oxidation state of palladium [35]. The Pd²⁺ peaks appear to be much more intense than GNPs peak, suggesting that gold nanoparticles are covered with a new layer of palladium composition. This is in agreement with both the XRD results and the TEM images, supporting formation of a core-shell like structure of Au@Pd.

After hydrogen exposure to colloidal solution of sample Au₁Pd₂, a significant shift for Pd_{3d} peaks occurs from 334.3 to

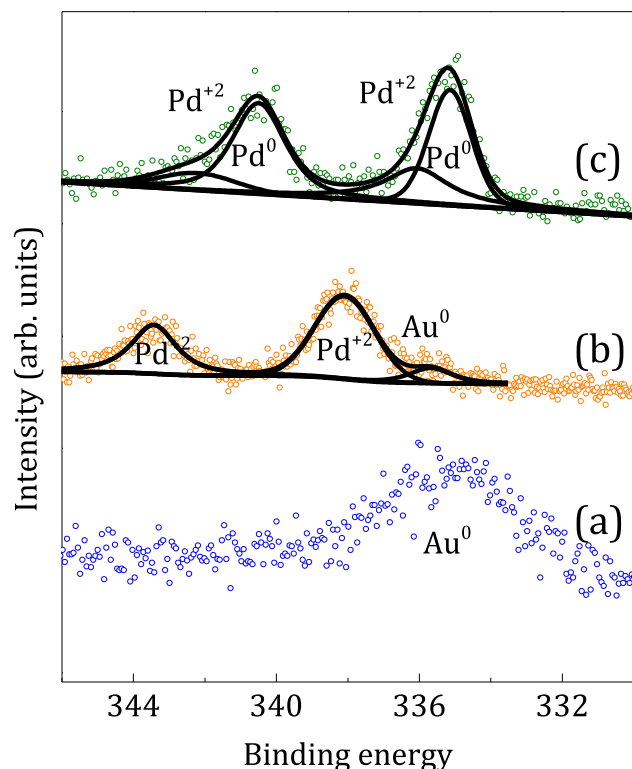


Fig. 4 – Typical Pd_{3d} high resolution XPS spectra of (a) pristine GNPs, (b) Au₁Pd₂ sample before and (c) after exposing to hydrogen gas.

338.1 eV towards lower binding energies of 335.1–340.5 eV, indicating reduction of Pd²⁺ states to Pd⁰ [35]. However, a part of the palladium remains in the Pd²⁺ oxidation state, which can be related to the formation of surface states of palladium oxide. Moreover, due to this peak shift, the Au_{4d} is no longer distinguishable and therefore has not been shown. XPS measurement on other Pd concentrations was also confirmed formation of metallic Pd after hydrogenation (not shown here).

The results presented above obviously indicate that addition of PdCl₂ solution into the GNPs, produced by laser ablation method, leads to attachment of palladium phases around the GNPs as a core-shell like structure. Indeed, GNPs have negative surface charges, so they attract palladium ions (Pd²⁺) with positive charges and are gradually covered by a layer of palladium [36–38]. Therefore, this result is also expected for gold nanoparticles prepared by other simple and inexpensive GNPs chemical synthesis methods. Various papers have reported the structure of the Pd–Au core-shell nanostructures based on Pd²⁺ ion precursors [39–45]. In these reports, galvanic displacement by another ion, such as copper, is often used to make a strong bond between the two phases. But in the case of our work, we want the shell to attach weakly to the core so that it can be separated easily by hydrogen recovery and affects the LSPR intensity or wavelength. Hydrogen exposure has a significant effect on the palladium shell in which the morphology is greatly changed and conversion to metallic Pd occurs. TEM suggests that the Pd²⁺ shells are removed from the GNPs as result of neutralization due to hydrogen induced conversion into the metallic Pd phase.

Cyclic voltammetry

To study the hydrogen absorption and desorption ability of samples, CV was used for pristine GNPs, PdCl₂ and sample Au₁Pd₂ before and after hydrogen exposure. In the CV curve of pristine GNPs (Fig. 5(a)), peak I (−0.2 V) is related to absorbed hydrogen from the H₂SO₄ electrolyte, peaks II (0.44 V) and III (0.9 V) are related to the formation of Au oxides and peaks IV (0.07 V) and V (0.49 V) correspond to reduction of the Au oxides during the cathodic scan [46,47]. In Fig. 5(b), CV of PdCl₂ was examined for comparison where peaks I, II and VII are related to the hydrogen adsorption/desorption region that absorbs from the electrolyte. Since PdCl₂ is a good precursor catalyst for hydrogen [48], these peaks are sharper than those of GNPs. Meanwhile, peaks III and IV are related to the formation of PdH_x, and peaks V and VI are related to the reduction of Pd ions to metallic Pd. Actually, the hydrogen adsorption/desorption occurs at the potential interval of −0.2 to 0.2 V, and oxidation and reduction occurs at 0.44–0.8 V and 0.3–0.5 V, respectively [49,50]. For the Au₁Pd₂ sample (black curve in part (c)), a combination of the signals of both GNPs and PdCl₂ are recognized. The separate of signals is not easy due to the overlap of the peaks. The last two cases was observed (Fig. 5(c)). However, after the hydrogen exposure (red line), oxidation and reduction peaks of GNPs are observable again, which somehow confirms the TEM images where PdCl₂ is converted and the GNPs are removed from the core-shell like morphology.

Optical absorption properties

Fig. 6 illustrates the optical absorption spectra of pristine GNPs, unexposed and hydrogen exposed sample Au₁Pd₂. LSPR peak of gold is located at 522 nm which undergoes a red-shift to 526 nm and its intensity lowers by adding PdCl₂ in Au₁Pd₂ sample. This spectral shift is attributed to the accumulation of a PdCl₂ agglomerates around the GNPs as shown in Fig. 3(b). The presence of PdCl₂ solution is also recognizable by arising the characteristic absorption peaks in 200–260 nm range.

Hydrogen exposure obviously causes the disappearance of the PdCl₂ absorption peak, as well as evolution of gold LSPR peak in terms of shape and position. These observations suggest a chemical reduction of PdCl₂ into metallic Pd occurs after hydrogen exposure, followed by a change in the refractive index of the GNPs' surrounding hence LSPR spectral shifting and variation. The LSPR peak can be describe theoretically by Drude model. In this model, the resonance frequency is obtained by the complex dielectric function of the material, ϵ , dielectric constant of nanoparticle medium, ϵ_m , the size and shape of nanoparticle [34]. The dipole polarizability, α , of a spherical small nanoparticle with diameter very smaller than the incident light wavelength is written as:

$$\alpha = 3\epsilon_0 V \left(\frac{\epsilon - \epsilon_m}{\epsilon + 2\epsilon_m} \right) \quad (1)$$

where V is the volume of the nanoparticle and ϵ_0 is vacuum permittivity. It is clear from the above equation that dipolar LSPR occurs when we have:

$$\epsilon_r = -2\epsilon_m \quad (2)$$

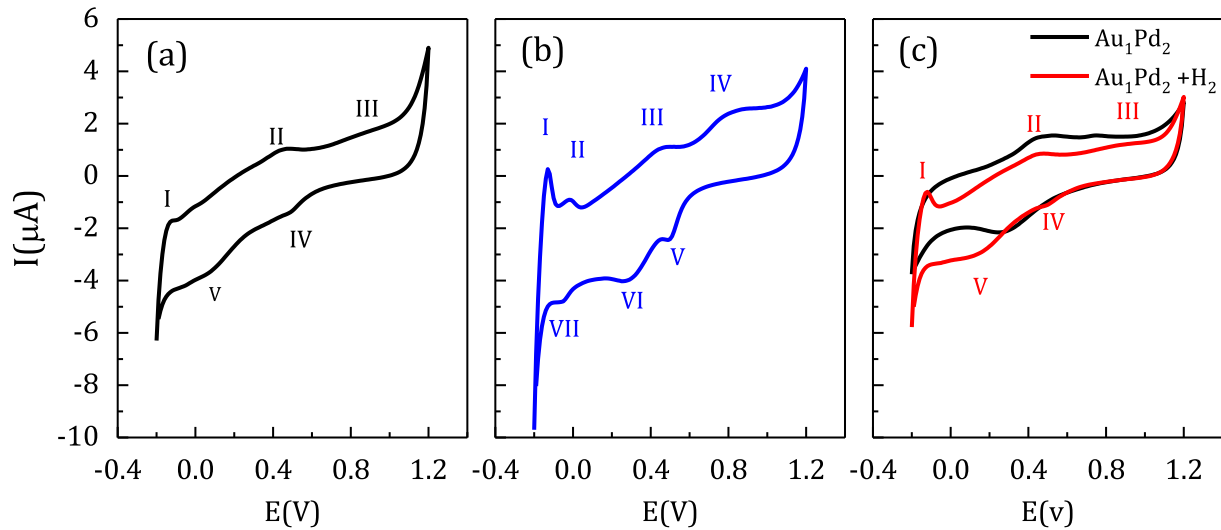


Fig. 5 – Cyclic voltammograms of (a) pristine GNPs (sample Au), (b) PdCl_2 and (c) sample Au_1Pd_2 before and after hydrogen exposure.

where ϵ_r is the real part of ϵ and can be expressed as a function of the frequency, ω :

$$\epsilon_r = 1 - \frac{\omega_p^2}{\omega^2 + \gamma^2} \quad (3)$$

where ω_p is the bulk plasma oscillation frequency (ratio of free carrier density and the electron effective mass) and γ is their bulk collision frequency which indicate the information of the electron scattering by the electron, hole, grain boundaries and the other scattering sources. From (2) and (3) we obtain the resonance frequency ω_{sp} , described by equation (4):

$$\omega_{sp} = \sqrt{\frac{\omega_p^2}{1 + 2\epsilon_m} - \gamma^2} \quad (4)$$

ω_{sp} represents the LSPR energy and γ is the damping constant due to electron collisions which for most metals assuming

minimal damping ($\gamma \approx 0$). Converting from ω_{sp} to λ_{sp} , we can rewrite the equation as:

$$\lambda_{sp} = \lambda_p \sqrt{1 + 2\epsilon_m} \quad (5)$$

Eq. (5) clearly shows that the plasmon resonance wavelength position for a metal nanoparticle is directly proportional to the permittivity or the refractive index, n_m , of the surrounding medium (where $n_m = \sqrt{\epsilon_m}$) [51,52]. Therefore, a change in the refractive index of the environment can be directly measured from the shift in the nanoparticles absorption spectra. When hydrogen intercalates into the Pd^{2+} shell converts it into the metallic Pd and causes its removal, the ϵ_m changes back near to that of water and lead to frequency variation [53].

According to the data collection shown above, it can be expected that the Au–Pd system is a good candidate compound for an LSPR-based hydrogen sensing with desirable sensitivity. For this purpose, we further examine the effect of hydrogen on Au–Pd samples with different Au: Pd ratio in the following.

LSPR hydrogen sensing

Fig. 7(a–e) left panel shows the optical absorption spectra of different Au–Pd samples before and after exposure of different hydrogen concentration (0–10%) in the range of 200–270 nm related to PdCl_2 characteristic absorption peaks. It can be clearly seen that the palladium absorption peaks decrease in the presence of hydrogen and then completely disappears by increasing hydrogen concentration to 10%. According to the Beer-Lambert law ($A = \epsilon lc$, where A is optical absorption, ϵ is absorptivity of the species in solution, l is optical path length and c is the species concentration) expressing that a solution concentration is proportional to its absorption [54], this represents a decrease in the concentration of PdCl_2 due to hydrogen-induced $\text{Pd}^{2+} \rightarrow \text{Pd}^0$ conversion.

Fig. 7(a–e) right panel shows the corresponding gold LSPR absorption spectra for the different Au–Pd samples under

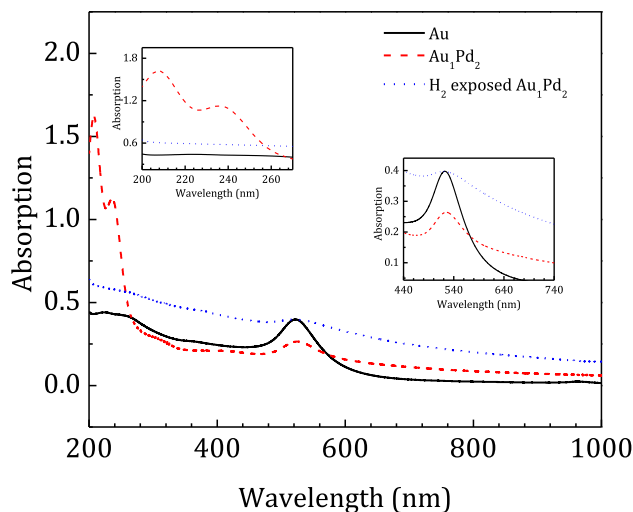


Fig. 6 – Optical absorption spectra of pristine GNPs (sample Au), sample Au_1Pd_2 before and after 10% H_2 exposure.

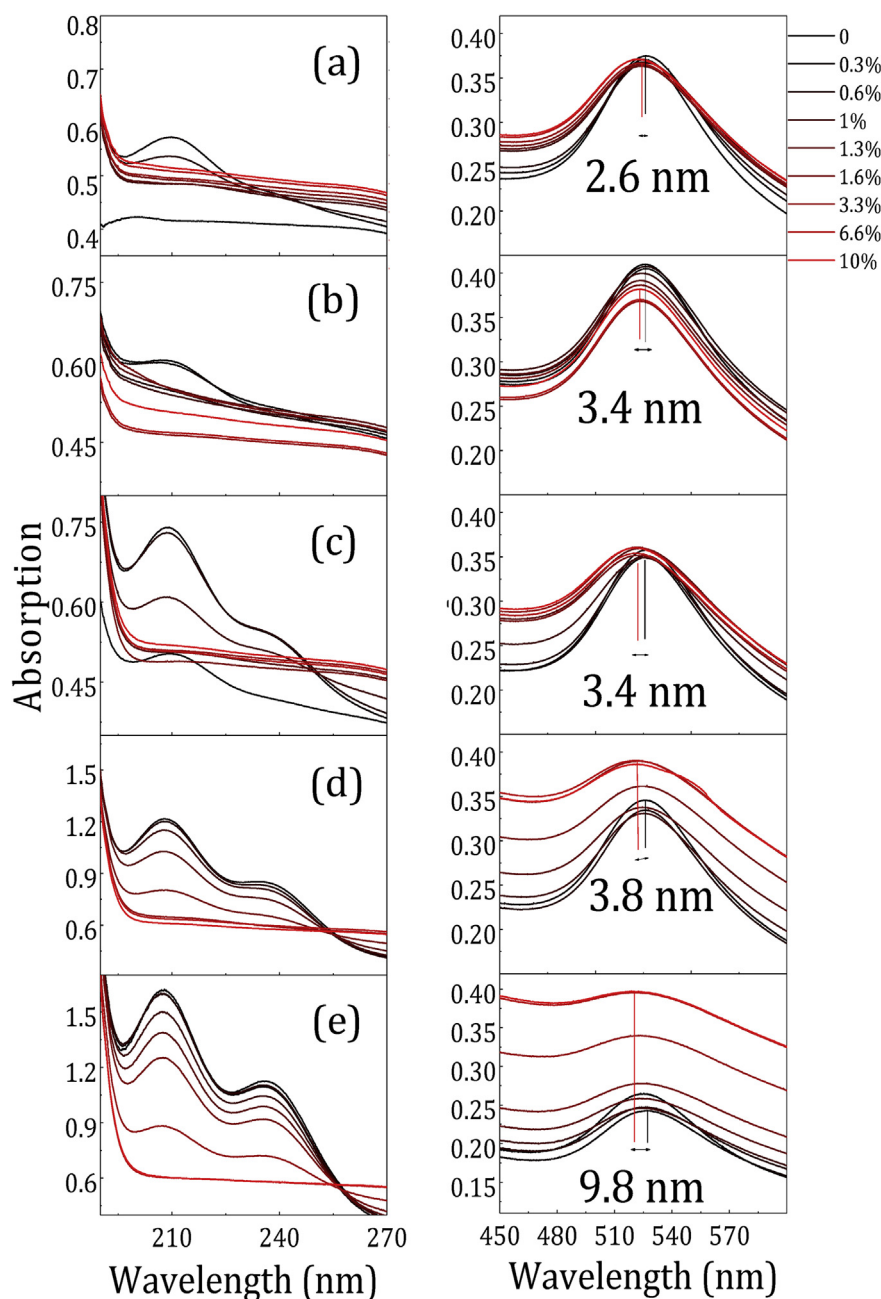


Fig. 7 – The effect of injection different hydrogen concentrations on the optical absorption spectra of various samples: (a) Au_8Pd_1 , (b) Au_4Pd_1 , (c) Au_2Pd_1 , (d) Au_1Pd_1 and (e) Au_1Pd_2 in the 190–270 nm range (left panel for absorption of PdCl_2) and 450–600 nm range (right panel for LSPR absorption of gold). (For interpretation of the references to color in this figure legend, the reader is referred to the Web version of this article.)

exposure of various concentration of hydrogen gas. The interaction of hydrogen with the colloidal samples causes a spectral evolution, both in terms of intensity and peak position. From the figure, in the low PdCl_2 content, the LSPR intensity reduces by increasing gas concentration. At higher PdCl_2 content (samples Au_1Pd_1 and Au_1Pd_2), however, one can see a significant increase in the overall intensity of the entire spectrum. This is attributed to the formation of slightly dark Pd NPs. Formation of Pd NPs causes significant blue shift and broadening of the LSPR peak. These shifts are 2.6, 3.4, 3.4, 3.8 and 9.8 nm for Au_8Pd_1 , Au_4Pd_1 , Au_2Pd_1 , Au_1Pd_1 and Au_1Pd_2

sample, respectively, indicating that a higher PdCl_2 gives a greater shift.

TEM imaging (not shown here) has shown that an increase in the proportion of Pd leads to a greater accumulation of Pd around the GNPs and to a greater thickness. However, investigating the true impact of thickness on the gas response requires more detailed analysis.

In the following, we focus on the correlation between gold LSPR shift, PdCl_2 absorption and gas concentration as is more meaningful in the plasmonic sensing mechanism. Fig. 8 (left panel) shows the LSPR wavelength position and PdCl_2

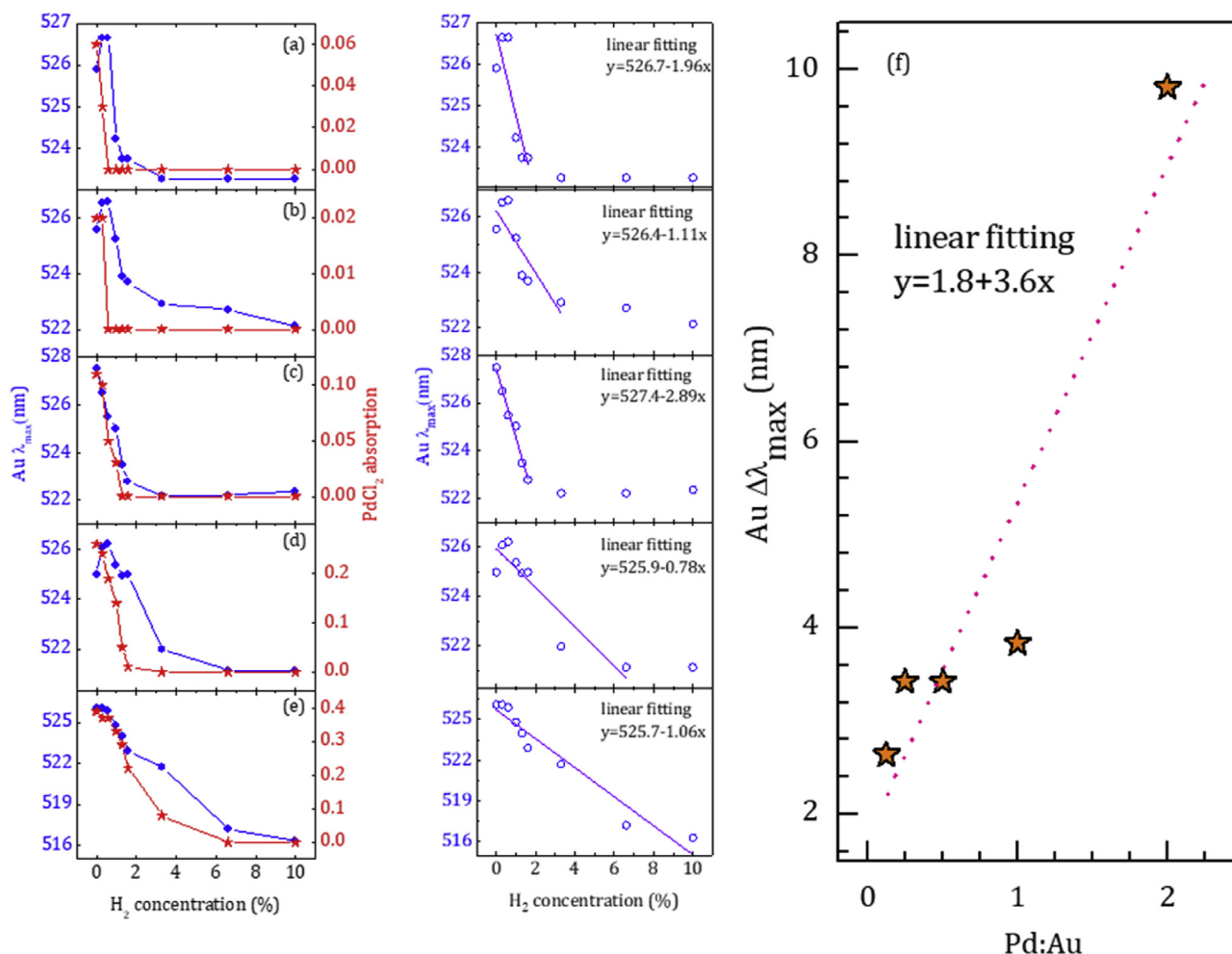


Fig. 8 – Left panel: gold LSPR peak position and PdCl₂ absorption peak intensity as a function of hydrogen concentration (0.3–10%) for (a) Au₈Pd₁, (b) Au₄Pd₁, (c) Au₂Pd₁, (d) Au₁Pd₁ and (e) Au₁Pd₂ samples. Middle panel: linear fittings and equations of LSPR peak position and (f) Au LSPR blue shift at 10% H₂ in terms of Pd:Au molar ratio.

absorption as a function of hydrogen concentration. As clearly seen, except for some initial wavelength increase in some samples, both the wavelength position and PdCl₂ absorption almost reduce and saturated with increasing H₂ concentration in a same manner suggesting a very close correlation between the gold LSPR wavelength and PdCl₂ absorption (or concentration). For example, sample Au₈Pd₁ in 1.3% and sample Au₁Pd₂ in 10% reach their saturation. The next noticeable point to be noted, shown in the middle panel of the figure, is the desirable detection capability with a good linearity for low concentrations of hydrogen (<4% range, the hydrogen explosion limit) based on LSPR shift with a possible large number of points. Although increasing the Pd:Au ratio (sample Au₁Pd₂) provides greater wavelength shift, sample Au₂Pd₁ (Fig. 8(c)) seems to exhibit a more linearity behavior among the other samples suggesting Pd:Au ratio should be optimized to have a more desirable sensing response. In addition, based on part (f), a linear relationship is observed between the blue shift and Pd:Au ratio, suggesting that by increasing the amount of PdCl₂ in the sample, more hydrogen is needed for the conversion process.

Despite the ability of our colloidal solution to detect low concentration of hydrogen, they are not reversible because the chemical composition of Pd²⁺ components could not be

return to their initial state. However, it can be utilized as disposable hydrogen detectors. It should be noted that, the LSPR sensing data are presented after making a large number of samples and ensuring their reproducibility. Although tolerance was observed in spectral shift in reproducibility studies, the overall behavior of samples was similar for hydrogen plasmonic resonance. The existing tolerance is expected to be minimized by controlling the particle size distribution and synthesize them more uniform.

One of the most important advantages of plasmonic hydrogen detection is the high accuracy due to the calibration capability based on the possible large number of data at low concentrations, which is evident in both our samples (Pd₂+Au system) and reported articles on Pd/Au [5,25–28]. Despite its disposability, the use of Pd₂+Au system seems is able to extend the hydrogen detection interval to higher range (10% in our case) which is rarely reported in Pd/Au system. For example, the Jiang reported a possible great accuracy under just 1% hydrogen concentration [5].

One of the disadvantages of our system that needs to be further studied is the low plasmonic shift compared to other papers [28]. The cause of this issue can be examined in two ways. First, because of the spherical gold particles,

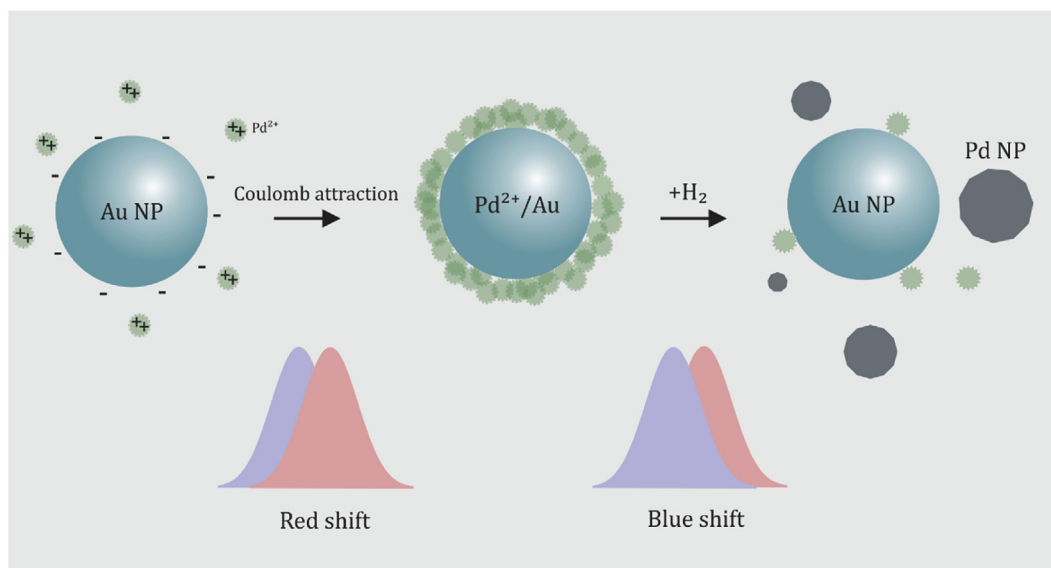


Fig. 9 – Schematic representation of LSPR hydrogen sensing mechanism in Pd^{2+}/Au system. Pd^{2+} cations are attracted by coulomb attraction force to the surface of GNPs for which a red-shift is observed. By hydrogen injection, Pd^{2+} states are reduced to metallic Pd which leave GNPs and a blue-shift occurs for gold LSPR peak. A small part of PdCl_2 may remain around the GNP. (For interpretation of the references to color in this figure legend, the reader is referred to the Web version of this article.)

longitudinal plasmonic modes are not activated. These modes usually show larger shifts and are observed in gold nanorods. For this reason, semiconductor plasmon particles with NIR LSPR have also been recently explored [20,55,56]. Second, due to poor bonding between the core and the shell, the change in the dielectric coefficients of the gold environment is not effective. Perhaps using a middle layer may overcome this problem.

LSPR hydrogen sensing mechanism

The mechanism of LSPR gas sensing is schematically shown in Fig. 9. In this model, after adding PdCl_2 solution (in which Pd^{2+} cations exist), the surface negative charges of GNPs absorb palladium ions by the coulomb attraction force. Then a layer of Pd^{2+} is formed around the GNPs (see the TEM images). The accumulation of these particles causes the change in the dielectric properties of GNPs adjacent and leads to a red-shift in LSPR peak. In the next step, with the injection of hydrogen gas, this Pd^{2+} layer reduces to metallic Pd NPs by a reduction reaction of:



And as a result, the coulomb attraction force is eliminated. This causes the newly-formed Pd NPs to be separated from the GNPs and bare GNPs are obtained again. As a result, the LSPR absorption peak undergoes a blue-shift. As our data showed, this spectral shifts were correlated with the ratio of palladium to gold, and in particular the concentration of hydrogen gas. This could be a good candidate for the LSPR-based hydrogen gas sensor. However, the selectivity of this sensing platform may be a challenges because the starting point of the sensing mechanism is reduction of Pd^{2+} ions and different reductant gases and chemicals are able to do it.

Conclusions

Pd^{2+}/Au core-shell like colloidal NPs were prepared by simple mixing of PdCl_2 solution and colloidal GNPs prepared by laser ablation method in water. As a result of mixing, Pd^{2+} ions are attracted on surface of GNPs and from a core-shell like morphology. The core-shell like Au@Pd^{2+} system is very sensitive to injection of low concentrations of hydrogen gas as it can convert Pd^{2+} into metallic palladium nanoparticles and make the GNPs free again. A strong correlation between gold LSPR position and PdCl_2 concentration by hydrogen gas was observed. This system showed a good ability toward LSPR detection of hydrogen gas below 4% with a possible large number of point.

Acknowledgement

The authors would like to thank the Iranian National Science Foundation (INSF) for their financial support.

REFERENCES

- [1] Sakintuna B, Lamari-Darkrim F, Hirscher M. Metal hydride materials for solid hydrogen storage: a review. *Int J Hydrogen Energy* 2007;32:1121–40. <https://doi.org/10.1016/j.ijhydene.2006.11.022>.
- [2] Guy KWA. The hydrogen economy. *Process Saf Environ Prot* 2000;78:324–7. <https://doi.org/10.1205/095758200530709>.
- [3] Ramanathan M, Skudlarek G, Wang HH, Darling SB. Crossover behavior in the hydrogen sensing mechanism for palladium ultrathin films. *Nanotechnology* 2010;21:125501. <https://doi.org/10.1088/0957-4484/21/12/125501>.

- [4] Chan CC, Hsu WC, Chang CC, Hsu CS. Hydrogen incorporation in gasochromic coloration of sol-gel WO₃ thin films. *Sens Actuators B Chem* 2011;157:504–9. <https://doi.org/10.1016/j.snb.2011.05.008>.
- [5] Jiang R, Qin F, Ruan Q, Wang J, Jin C. Ultrasensitive plasmonic response of bimetallic Au/Pd nanostructures to hydrogen. *Adv Funct Mater* 2014;24:7328–37. <https://doi.org/10.1002/adfm.201402091>.
- [6] Khalil I, Julkapli NM, Yehye WA, Basirun WJ, Bhargava SK. Graphene-gold nanoparticles hybrid-synthesis, functionalization, and application in an electrochemical and surface-enhanced Raman scattering biosensor. *Materials* 2016;9:406. <https://doi.org/10.3390/ma9060406>.
- [7] Rusman NAA, Dahari M. A review on the current progress of metal hydrides material for solid-state hydrogen storage applications. *Int J Hydrogen Energy* 2016;41:12108–26. <https://doi.org/10.1016/j.ijhydene.2016.05.244>.
- [8] Sugawa K, Tahara H, Yamashita A, Otsuki J, Sagara T, Harumoto T, et al. Refractive index susceptibility of the plasmonic palladium nanoparticle: potential as the third plasmonic sensing material. *ACS Nano* 2015;9:1895–904. <https://doi.org/10.1021/nn506800a>.
- [9] Langhammer C, Zoric I, Kasemo B, Clemens BM. Hydrogen storage in Pd nanodisks characterized with a novel nanoplasmonic sensing scheme. *Nano Lett* 2007;7:3122–7. <https://doi.org/10.1021/nl071664a>.
- [10] Wadell C, Syrenova S, Langhammer C. Plasmonic hydrogen sensing with nanostructured metal hydrides. *ACS Nano* 2014;8:11925–40. <https://doi.org/10.1021/nn505804f>.
- [11] Yoshimura K, Langhammer C, Dam B. Metal hydrides for smart window and sensor applications. *MRS Bull* 2013;38:495–503. <https://doi.org/10.1557/mrs.2013.129>.
- [12] Kalanur SS, Heo J, Yoo IH, Seo H. 2-D WO₃ decorated with Pd for rapid gasochromic and electrical hydrogen sensing. *Int J Hydrogen Energy* 2017;42:16901–8. <https://doi.org/10.1016/j.ijhydene.2017.05.172>.
- [13] Slaman M, Dam B, Schreuders H, Griessen R. Optimization of Mg-based fiber optic hydrogen detectors by alloying the catalyst. *Int J Hydrogen Energy* 2008;33:1084–9. <https://doi.org/10.1016/j.ijhydene.2007.09.036>.
- [14] Qu J, Sun B, Liu Y, Yang R, Li Y, Li X. Improved hydrogen storage properties in Mg-based thin films by tailoring structures. *Int J Hydrogen Energy* 2010;35:8331–6. <https://doi.org/10.1016/j.ijhydene.2009.12.007>.
- [15] Liu Y, Chen J, Peng L, Deng N, Ding W. Fabrication and optical property improvement of gasochromic switchable mirror based on Pd/Mg[sbnd]Nb₂O₅ thin film. *Int J Hydrogen Energy* 2019;44:15205–17. <https://doi.org/10.1016/j.ijhydene.2019.04.099>.
- [16] Wang H, Gao G, Wu G, Zhao H, Qi W, Chen K, et al. Fast hydrogen diffusion induced by hydrogen pre-split for gasochromic based optical hydrogen sensors. *Int J Hydrogen Energy* 2019;44:15665–76. <https://doi.org/10.1016/j.ijhydene.2019.04.026>.
- [17] Westerwaal RJ, Rooijmans JSA, Leclercq L, Gheorghe DG, Radeva T, Mooij L, et al. Nanostructured Pd-Au based fiber optic sensors for probing hydrogen concentrations in gas mixtures. *Int J Hydrogen Energy* 2013;38:4201–12. <https://doi.org/10.1016/j.ijhydene.2012.12.146>.
- [18] Petryayeva E, Krull UJ. Localized surface plasmon resonance: nanostructures, bioassays and biosensing-A review. *Anal Chim Acta* 2011;706:8–24. <https://doi.org/10.1016/j.aca.2011.08.020>.
- [19] Hydrogen enriched water swellable clay having reduced acid demand and stable at low pH. *Int J Hydrogen Energy* 1985. [https://doi.org/10.1016/0360-3199\(85\)90124-7](https://doi.org/10.1016/0360-3199(85)90124-7).
- [20] Shafieyan AR, Ranjbar M, Kameli P. Localized surface plasmon resonance H₂ detection by MoO₃ colloidal nanoparticles fabricated by the flame synthesis method. *Int J Hydrogen Energy* 2019;44:18628–38. <https://doi.org/10.1016/j.ijhydene.2019.05.171>.
- [21] Mayer KM, Hafner JH, Antigen AA. Localized surface plasmon resonance sensors. 2011. p. 3828–57.
- [22] Stewart ME, Anderton CR, Thompson LB, Maria J, Gray SK, Rogers JA, et al. Nanostructured plasmonic sensors. *Chem Rev* 2008;108:494–521. <https://doi.org/10.1021/cr068126n>.
- [23] Simakin AV, Voronov VV, Kirichenko NA, Shafeev GA. Nanoparticles produced by laser ablation of solids in liquid environment. *Appl Phys A Mater Sci Process* 2004;79:1127–32. <https://doi.org/10.1007/s00339-004-2660-8>.
- [24] Scaramuzza S, Zerbetto M, Amendola V. Synthesis of gold nanoparticles in liquid environment by laser ablation with geometrically confined configurations: insights to improve size control and productivity. *J Phys Chem C* 2016;120:9453–63. <https://doi.org/10.1021/acs.jpcc.6b00161>.
- [25] Rodal-Cedeira S, Montes-García V, Polavarapu L, Solís DM, Heidari H, La Porta A, et al. Plasmonic Au@Pd nanorods with boosted refractive index susceptibility and SERS efficiency: a multifunctional platform for hydrogen sensing and monitoring of catalytic reactions. *Chem Mater* 2016;28:9169–80. <https://doi.org/10.1021/acs.chemmater.6b04941>.
- [26] Wadell C, Nugroho FAA, Lidström E, Iandolo B, Wagner JB, Langhammer C. Hysteresis-free nanoplasmonic Pd-Au alloy hydrogen sensors. *Nano Lett* 2015;15:3563–70. <https://doi.org/10.1021/acs.nanolett.5b01053>.
- [27] Wy Y, Lee S, Wi DH, Han SW. Colloidal clusters of bimetallic core-shell nanoparticles for enhanced sensing of hydrogen in aqueous solution. *Part Part Syst Charact* 2018;35:1700380. <https://doi.org/10.1002/ppsc.201700380>.
- [28] Chiu CY, Huang MH. Polyhedral Au-Pd core-shell nanocrystals as highly spectrally responsive and reusable hydrogen sensors in aqueous solution. *Angew Chem Int Ed* 2013;52:12709–13. <https://doi.org/10.1002/anie.201306363>.
- [29] Song H, Luo Z, Liu M, Zhang G, Peng W, Wang B, et al. Centrifugal deposited Au-Pd core-shell nanoparticle film for room-temperature optical detection of hydrogen gas. *Sensors (Switzerland)* 2018;18:1448. <https://doi.org/10.3390/s18051448>.
- [30] Nishijima Y, Shimizu S, Kurihara K, Hashimoto Y, Takahashi H, Balçytis A, et al. Optical readout of hydrogen storage in films of Au and Pd. *Opt Express* 2017;25:24081. <https://doi.org/10.1364/oe.25.024081>.
- [31] Yang GW. Laser ablation in liquids: applications in the synthesis of nanocrystals. *Prog Mater Sci* 2007;52:648–98. <https://doi.org/10.1016/j.pmatsci.2006.10.016>.
- [32] Tew MW, Miller JT, Van Bokhoven JA. Particle size effect of hydride formation and surface hydrogen adsorption of nanosized palladium catalysts: L3 Edge vs K Edge X-ray absorption spectroscopy. *J Phys Chem C* 2009;113:15140–7. <https://doi.org/10.1021/jp902542f>.
- [33] Sheykhirad Z, Ranjbar M, Farokhpour H, Salamati H. Direct fabrication of Au/Pd(II) colloidal core-shell nanoparticles by pulsed laser ablation of gold in PdCl₂ solution. *J Phys Chem C* 2015;119:9534–42. <https://doi.org/10.1021/jp512582q>.
- [34] Teixeira-Neto AA, Gonçalves RV, Rodella CB, Rossi LM, Teixeira-Neto E. Surface composition and structural changes on titanium oxide-supported AuPd nanoparticles during CO oxidation. *Catal Sci Technol* 2017;7:1679–89. <https://doi.org/10.1039/c7cy00137a>.
- [35] Kalhori H, Ranjbar M, Salamati H, Coey JMD. Flower-like nanostructures of WO₃: fabrication and characterization of their in-liquid gasochromic effect. *Sens Actuators B Chem* 2016;225:535–43. <https://doi.org/10.1016/j.snb.2015.11.044>.
- [36] Konda SK, Chen A. Palladium based nanomaterials for enhanced hydrogen spillover and storage. *Mater Today* 2016;19:100–8. <https://doi.org/10.1016/j.mattod.2015.08.002>.

- [37] Darroudi M, Ahmad MB, Zamiri R, Abdullah AH, Ibrahim NA, Sadrolhosseini AR. Time-dependent preparation of gelatin-stabilized silver nanoparticles by pulsed Nd:YAG laser. *Solid State Sci* 2011;13:520–4. <https://doi.org/10.1016/j.solidstatesciences.2010.12.018>.
- [38] Maciulevičius M, Vinciunas A, Brikas M, Butsen A, Tarasenko N, Tarasenko N, et al. Pulsed-laser generation of gold nanoparticles with on-line surface plasmon resonance detection. *Appl Phys A Mater Sci Process* 2013;111:289–95. <https://doi.org/10.1007/s00339-012-7535-9>.
- [39] Raghavendra P, Vishwakshan Reddy G, Sivasubramanian R, Sri Chandana P, Subramanyam Sarma L. Reduced graphene oxide-supported Pd@Au bimetallic nano electrocatalyst for enhanced oxygen reduction reaction in alkaline media. *Int J Hydrogen Energy* 2018;43:4125–35. <https://doi.org/10.1016/j.ijhydene.2017.07.199>.
- [40] Kunz S, Iglesia E. Mechanistic evidence for sequential displacement-reduction routes in the synthesis of Pd-Au clusters with uniform size and clean surfaces. *J Phys Chem C* 2014;118:7468–79. <https://doi.org/10.1021/jp500537v>.
- [41] Mandal S, Mandale AB, Sastry M. Keggin ion-mediated synthesis of aqueous phase-pure Au@Pd and Au@Pt core-shell nanoparticles. *J Mater Chem* 2004;14:2868–71. <https://doi.org/10.1039/b409033k>.
- [42] Huang X, Wu H, Pu S, Zhang W, Liao X, Shi B. One-step room-temperature synthesis of Au@Pd core-shell nanoparticles with tunable structure using plant tannin as reductant and stabilizer. *Green Chem* 2011;13:950–7. <https://doi.org/10.1039/c0gc00724b>.
- [43] Balcha T, Strobl JR, Fowler C, Dash P, Scott RWJ. Selective aerobic oxidation of crotyl alcohol using aupd core-shell nanoparticles. *ACS Catal* 2011;1:425–36. <https://doi.org/10.1021/cs200040a>.
- [44] Hsu C, Wei M, Wei Z, Liu F. Improving the catalytic activity of Au/Pd core-shell nanoparticles with a tailored Pd structure for formic acid oxidation reaction. *RSC Adv* 2016;6:24645–50. <https://doi.org/10.1039/c6ra02214f>.
- [45] Venkatesan P, Santhanalakshmi J. Core-shell bimetallic Au-Pd nanoparticles: synthesis, structure, optical and catalytic properties. *Nanosci Nanotechnol* 2012;1:43–7. <https://doi.org/10.5923/j.nn.20110102.08>.
- [46] Lertanantawong B, O'Mullane AP, Surareungchai W, Somasundrum M, Burke LD, Bond AM. Study of the underlying electrochemistry of polycrystalline gold electrodes in aqueous solution and electrocatalysis by large amplitude fourier transformed alternating current voltammetry. *Langmuir* 2008;24:2856–68. <https://doi.org/10.1021/la702454k>.
- [47] Diamond D. *Analytical electrochemistry*, vol. 15. New York: John Wiley & Sons; 1996. [https://doi.org/10.1016/s0165-9936\(96\)90116-8](https://doi.org/10.1016/s0165-9936(96)90116-8).
- [48] Morisse CGA, McInroy AR, Anderson C, Mitchell CJ, Parker SF, Lennon D. Structure/activity relationships applied to the hydrogenation of α,β -unsaturated carbonyls: the hydrogenation of 3-butyne-2-one over alumina-supported palladium catalysts. *Catal Today* 2017;283:110–8. <https://doi.org/10.1016/j.cattod.2016.02.028>.
- [49] Abys JA, Dullaghan CA. *Electrodeposition of palladium and palladium alloys*. *Mod Electroplat* 2000;327–68.
- [50] Soreta TR, Strutwolf J, O'Sullivan CK. Electrochemically deposited palladium as a substrate for self-assembled monolayers. *Langmuir* 2007;23:10823–30. <https://doi.org/10.1021/la7006777>.
- [51] Luther JM, Jain PK, Ewers T, Alivisatos AP. Localized surface plasmon resonances arising from free carriers in doped quantum dots. *Nat Mater* 2011;10:361–6. <https://doi.org/10.1038/nmat3004>.
- [52] Ghosh SK, Pal T. Interparticle coupling effect on the surface plasmon resonance of gold nanoparticles: from theory to applications. *Chem Rev* 2007;107:4797–862. <https://doi.org/10.1021/cr0680282>.
- [53] Mitra S, Chattopadhyay R, Bhadra SK. Modelling of Palladium Gold alloy- dielectric stratified loaded plasmonic waveguide for hydrogen detection at room temperature. *J Phys Conf Ser* 2016;759. <https://doi.org/10.1088/1742-6596/759/1/012043>.
- [54] Takahashi H, Okazaki S, Nishijinia Y, Arakawa T. Optimization of hydrogen sensing performance of Pt/WO₃ gasochromic film fabricated by sol-gel method. *Sens Mater* 2017;29:1259–68. <https://doi.org/10.18494/SAM.2017.1585>.
- [55] Nugroho FAA, Darmadi I, Cusinato L, Susarrey-Arce A, Schreuders H, Bannenberg LJ, et al. Metal-polymer hybrid nanomaterials for plasmonic ultrafast hydrogen detection. *Nat Mater* 2019;18:489–95. <https://doi.org/10.1038/s41563-019-0325-4>.
- [56] Zhao Y, Pan H, Lou Y, Qiu X, Zhu J, Burda C. Plasmonic Cu 2-xS nanocrystals: optical and structural properties of copper-deficient copper(I) sulfides. *J Am Chem Soc* 2009;131:4253–61. <https://doi.org/10.1021/ja805655b>.